Determination of the Partial Structure Factors of Amorphous CuZr by Anomalous X-Ray Scattering and Reverse Monte Carlo

M. Bionducci[a], F. Buffa[a], G. Licheri[a], G. Navarra[a], B. Bouchet-Fabre[b], and J. M. Tonnerre[c]

[a] Dipartimento di Scienze Chimiche, Università di Cagliari, via Ospedale 72, I-09124 Cagliari
[b] LURE, Bâtiment 209 D, Université de Paris-Sud, F-91405 Orsay Cedex
[c] Laboratoire de Cristallographie CNRS, av. des Martyrs, F-38042 Grenoble

Z. Naturforsch. **51a**, 71–82 (1996); received November 15, 1995

Anomalous X-ray Scattering experiments have been performed to study the local order in an amorphous CuZr sample prepared by mechanical alloying. The three partial structure factors were extracted both using a regularization algorithm to solve an ill-conditioned system of linear equations and applying the reverse Monte Carlo technique to the experimental data. Then the short range atomic distributions of similar samples prepared by different methods and investigated by different techniques are compared.

Key words: Amorphous Alloys, Anomalous X-ray Scattering, Regularization Algorithm, Reverse Monte Carlo, Partial Structure Factors.

1. Introduction

The unusual physical and chemical properties of non-crystalline alloys have motivated, in the last years, the development of new techniques for producing amorphous materials. At the same time, the short-range atomic environment of these metastable compounds has extensively been studied and a new branch of science emerged: *amorphography* [1]. How far is the amorphous state from thermodynamic equilibrium? Has every amorphous specimen its own atomic structure or can its structure be considered a slight modification from an *ideal glass state*? To elucidate the latter point, it is necessary to compare high quality experimental information about the atomic distribution of different samples.

In the simple case of binary systems it is possible to obtain a good description of the atomic structure by extracting the three partial structure factors (PSFs). This requires three different experiments which involve strong contrast among the atomic form factors [2]. When suitable isotopes are available, the neutron scattering technique may be used to obtain the PSFs [3]. Unfortunately, it can be applied to only a few elements.

On the other hands, thanks to the tunability, high brightness and intensity of synchrotron radiation it is possible to take advantage of the energy dependence of the X-ray scattering factors (anomalous X-ray scattering, AXS [4]). However, even for binary compounds the system of linear equation is ill-conditioned and the solutions are strongly sensitive to small changes in the data. The presence of both random and systematic errors could prevent a good solution and standard least-squares routines often fail to provide a solution with physical meaning. Different non-standard methods for solving the ill-conditioned system have been proposed [5–9].

In this paper we describe the application of the AXS technique to extract the PSFs of CuZr amorphous alloy prepared by mechanical alloying. Preliminary results have been reported in [10]. A regularization algorithm for treating the ill-conditioned system will be described. The comparison of the short range atomic arrangement with the structural parameters obtained from AXS [9, 11] and neutron scattering techniques [12, 13] on rapidly quenched samples is also discussed. Furthermore, the reverse Monte Carlo (RMC) technique has been used to obtain an independent set of PSFs and partial distribution functions (PDFs) that best reproduce the experimental functions.

2. Formalism and Strategies

2.1. Scattering Formalism

According to the Faber-Ziman formalism [14], the total structure factor (TSF) $a(q, E)$, for a binary amor-

Reprint requests to Prof. G. Licheri,
E-mail: Licheri@Vaxca2.Unica.It.

0932-0784 / 96 / 0100-0071 $ 06.00 © – Verlag der Zeitschrift für Naturforschung, D-72072 Tübingen

phous system, can be defined as a weighted sum of three PSFs, $a_{ij}(q)$, [15, 16]:

$$a(q, E) = w_{AA}(q, E)\, a_{AA}(q) + 2\, w_{AB}(q, E)\, a_{AB}(q) + w_{BB}(q, E)\, a_{BB}(q), \quad (1)$$

$$w_{ij}(q, E) = c_i c_j f_i f_j^* / \langle f \rangle^2, \quad (2)$$

$$\langle f \rangle^2 = | c_A f_A + c_B f_B |^2, \quad (3)$$

where c_i and $f_i = f_i(q, E)$ are the concentration and the atomic scattering factor of species i, respectively.

The X-rax atomic scattering factor can be written as

$$f_i(q, E) = f_i^0(q) + f_i'(q, E) + i\, f_i''(q, E), \quad (4)$$

where $q = 4\pi \sin(\vartheta)/\lambda$ is the modulus of the scattering vector with 2ϑ the scattering angle and λ the photon wavelength, E is the photon energy, f_i^0 the Fourier transform of the electron density, and f_i' and f_i'' are the real and imaginary parts of the anomalous dispersion correction, respectively. The dependence of these terms of the scattering angle is negligible, but they change abruptly when the energy of the incident beam is tuned near the absorption edge of the i species.

For PSF available in the reciprocal space in the range from q_1 to q_2, the partial pair correlation function, $G_{ij}(r)$, is defined as

$$G_{ij}(r) = \frac{2}{\pi} \int_{q_1}^{q_2} q\, [a_{ij}(q) - 1] \sin(qr)\, \mathrm{d}q. \quad (5)$$

The nearest neighbour distances R_{ij} are given by the position of the first maximum in the $G_{ij}(r)$. The PDFs can be calculated from

$$\mathrm{PDF}_{ij}(r) = c_j [4\pi \varrho_0 r^2 + r\, G_{ij}(r)], \quad (6)$$

ϱ_0 being the mean atomic number density. The number of j atoms around the atomic species i in the range from r_1 to r_2 can be evaluated as

$$N_{ij} = \int_{r_1}^{r_2} \mathrm{PDF}_{ij}(r)\, \mathrm{d}r. \quad (7)$$

To evaluate the chemical ordering, the parameter η_{AB} proposed by Cargill and Spaepen [17] may be adopted:

$$\eta_{AB} = N_{AB}/N_{AB}^* - 1, \quad (8)$$

where $N_{AB}^* = c_B N_A N_B / \langle N \rangle$, $N_i = N_{ii} + N_{ij}$ and $\langle N \rangle = c_A N_A + c_B N_B$.

2.2. *Differential Anomalous Scattering (DAS)*

The first step to separate the PSFs is reached by calculating the differential structure factors (DSFs) around each atomic species present in the sample. A differential structure factor can be obtained by performing scattering experiments at two energies, respectively near and far from the absorption edge of an element. By taking the difference between these two data sets, all correlations not involving the chosen atom disappear:

$$\mathrm{DSF}_A(q, E_1, E_2) = \Delta w_{AA}\, a_{AA}(q) + \Delta w_{AB}\, a_{AB}(q), \quad (9)$$

$$\Delta w_{ij}(q, E_1, E_2) = [w_{ij}(q, E_1) \langle f(E_1) \rangle^2 - w_{ij}(q, E_2) \langle f(E_2) \rangle^2] / [\langle f(E_1) \rangle^2 - \langle f(E_2) \rangle^2], \quad (10)$$

the coefficient Δw_{BB} being practically zero.

The Fourier sine transform of DSF_A gives the differential distribution function $\mathrm{DDF}_A(r)$, which describes the structure around the atom A. Therefore it is sensitive only to the environment of that atom:

$$\mathrm{DDF}_A(r, E_1, E_2) = \frac{2}{\pi} \int_{q_1}^{q_2} q\, [\mathrm{DSF}_A(q, E_1, E_2) - 1] \sin(qr)\, \mathrm{d}q, \quad (11)$$

With a suitable choice of the difference between the two energies (i.e., a large enough difference to yield a significant change in f' but not too large, so that one can assume that the two measurements have been performed under similar experimental conditions), the DAS procedure is able to partially cancel some systematic errors.

This technique provides local information similar to that provided by Extended X-ray Absorption Fine Structure (EXAFS) technique. These two techniques are complementary because they cover different ranges of the reciprocal space [18].

2.3. *Strategies for Obtaining the PSFs*

2.3.1. Anomalous X-Ray Scattering (AXS)

The three partial structure factors can, in principle, be determined using three independent measurements with varying f_i and solving, for each q-value, a system of linear equations. In matrix notation:

$$\mathbf{W}\boldsymbol{p} = \boldsymbol{t}, \quad (12)$$

where the elements of the vector $\boldsymbol{t}$ are the measured TSFs, $a(q, E)$; $\boldsymbol{p}$ is the unknown vector of the PSFs $a_{ij}(q)$ and $\mathbf{W}$ is the matrix of the weighting coefficients $w_{ij}(q, E)$.

Unfortunately, this system is ill-conditioned due to very weak differences among its rows, and the solution

is strongly sensitive to small changes in the data vector, $\boldsymbol{t}$. Consequently, the noise or the systematic errors present in $\boldsymbol{t}$ could prevent a correct solution.

The conditioning can be evaluated through the singular value decomposition (SVD) of the matrix $\mathbf{W}$. As known [19], the SVD of a matrix $\mathbf{W}(m, n)(m > n)$ gives two orthogonal matrices $\mathbf{U}$, $\mathbf{V}$ and a diagonal matrix $\mathbf{D}$, such that

$$\mathbf{W} = \mathbf{U}\mathbf{D}\mathbf{V}^{\mathrm{T}}; \quad \mathbf{U}^{\mathrm{T}}\mathbf{U} = \mathbf{I}_m, \quad \mathbf{V}^{\mathrm{T}}\mathbf{V} = \mathbf{I}_n, \tag{13}$$

$$\mathbf{D} = \mathrm{diag}(\sigma_1, \sigma_2, \ldots, \sigma_n), \tag{14}$$

$$\sigma_1 \geq \sigma_2 \geq \ldots \geq \sigma_n \geq 0. \tag{15}$$

In (13) $\mathbf{I}_m$ and $\mathbf{I}_n$ are the identity matrices of order m and n, respectively, and the elements, σ_l, of the diagonal matrix, $\mathbf{D}$, are the singular values of the matrix $\mathbf{W}$. The ratio between the first and the last non-zero singular value is called the conditioning number of $\mathbf{W}$, $\mathrm{cond}(\mathbf{W})$, and represents an amplification factor in propagating the experimental errors. Indeed, if $\boldsymbol{\delta t}$ is the error vector associated with $\boldsymbol{t}$, the relative error $\boldsymbol{\delta p}$ of the solution vector $\boldsymbol{p}$, is given by [20]

$$\| \delta \boldsymbol{p} \| / \| \boldsymbol{p} \| \leq \mathrm{cond}(\mathbf{W}) \| \delta \boldsymbol{t} \| / \| \boldsymbol{t} \|, \tag{16}$$

where $\| \ \|$ denotes the Euclidean norm. Typically, the value of $\mathrm{cond}(\mathbf{W})$ for AXS experiments is larger than that encountered in neutron scattering experiments using isotopic substitution.

Given the poor conditioning, a new approach is to introduce further information to decrease the condition number, this way making the system more stable. A strategy suggested by Munro [21] and implemented by Ludwig [22] and de Lima [5] consists in introducing in the system (12) the two differential structure factors, calculated near the K-edge of both elements. Really, the introduction of these functions represents an important improvement towards obtaining a stable solution of the system. The solution of the system is obtained, for each value of the scattering vector $\boldsymbol{q}$, by minimizing the quadratic function $\| \mathbf{W}p - t \|^2$. This strategy has been successfully applied in the study of amorphous Ni_2Zr, for which high quality data with a very low level of noise were available [23].

Nevertheless, often the decreasing of the conditioning number is not sufficient for obtaining a good solution. In these cases some regularization methods have been proposed to reduced the influence of the noise [7, 8]. In practice, the quadratic function to be minimized is

$$Q_\lambda^{[k]}(p) = \lambda \| \mathbf{H}^{[k]} p \|^2 + \| \mathbf{W}p - t \|^2, \tag{17}$$

where $\mathbf{H}^{[k]}$ is the regularization matrix and λ is the regularization parameter which determines the influence of the matrix $\mathbf{H}$. Following the usual procedures of regularization in Euclidean spaces, three different regularization matrices can be considered. Each of them corresponds to a different constraint being imposed on the regularized solution. The choice $k = 0$ corresponds to a control on the norm of the vector $\boldsymbol{p}$, i.e. it prevents the three components of $\boldsymbol{p}$ from becoming too large. The choices $k = 1$ and $k = 2$ correspond to a control on the first and second variations in the components of $\boldsymbol{p}$, respectively. The value of the regularization parameter must be carefully chosen: if λ is too large, the solution vector $\boldsymbol{p}$ does not correspond to the input data; on the other hand, if λ is too small $\boldsymbol{p}$ tends to the least-squares solution. This method has been demonstrated to have good properties of stability, in absence of systematic errors, even in the case of highly noisy data [7].

However, in experimental situations also systematic errors are usually present in the measured data. They are more dangerous than random errors, since they often vary slowly with q. The presence of systematic errors gives rise to some specularity (*mirror effect*) both in PSFs and in the PDFs [24]. In the reciprocal space the amplitude of the PSFs is often far from being physically meaningful. This fact causes, in real space, the presence of wide regions where the atomic distribution is negative. Although systematic errors are not successfully treated by the regularization algorithms, it is possible to rewrite the system (12) so that all q-points are simultaneously involved and the constraints are applied to consecutive points of the three PSFs at the same time [25, 26].

In experimental situations it is quite difficult to appreciate the level of systematic errors but, in some cases, the constraints are able to reduce their effects forcing the solutions, the PSFs and then the PDFs, to change simultaneously. This often leads, at varying λ, to a progressive reduction of unphysical behaviour and mirror effect. Therefore, the criterion of minimizing the presence of unphysical negative values in real space can be used to stop the regularization process.

The efficiency of the regularization algorithm was tested by comparing the regularized PDFs with those obtained with other methods. Figures 1 and 2 show the regularized PDFs at different values of the regularization parameter, for amorphous $NiZr_2$ and $NiZr_3$, respectively. In the case of the least-squares solution (curves a) only the Zr–Zr PDFs exhibit an

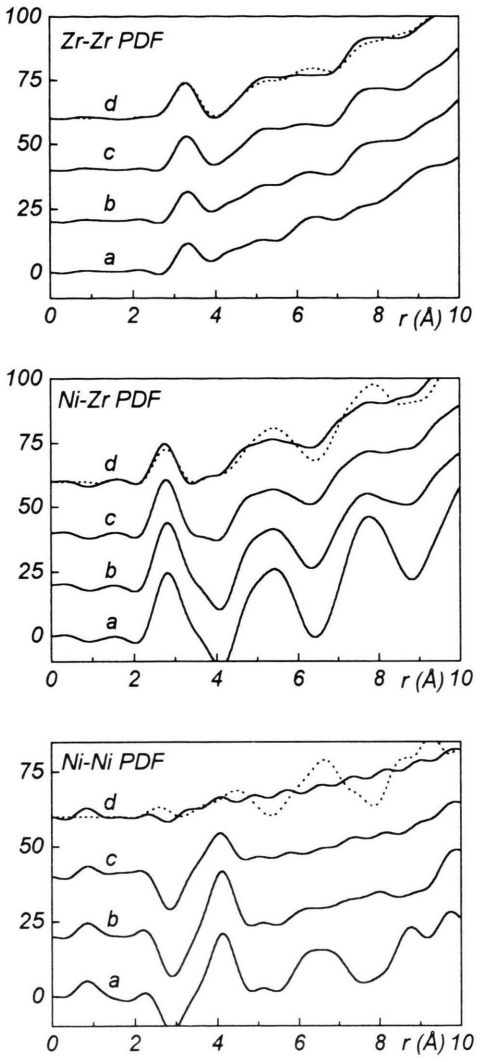

Fig. 1. Partial distribution functions for the amorphous $NiZr_2$ at increasing of the regularization parameter; curves (a): least-squares solution. Final curves (d) are compared with results obtained by applying an iterative method (dotted lines) [5].

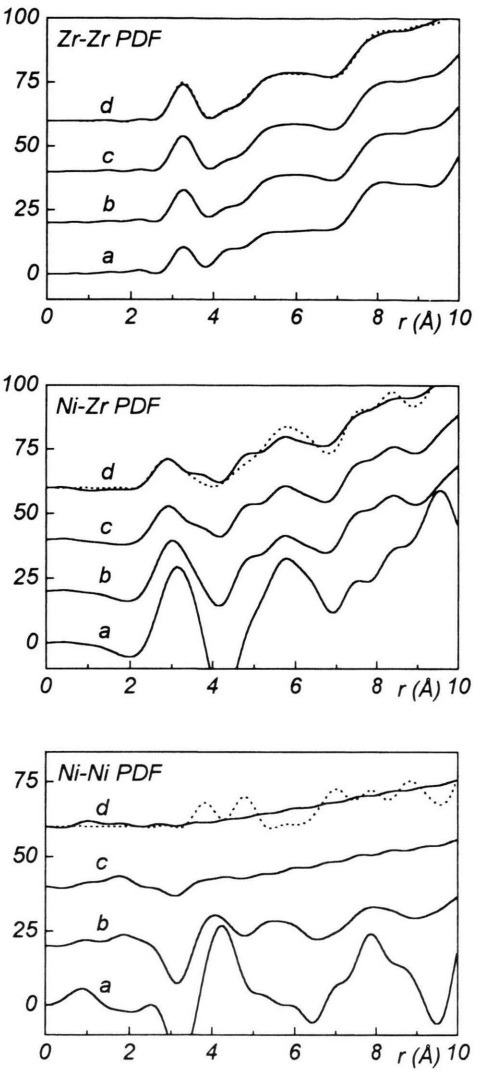

Fig. 2. Partial distribution functions for the amorphous $NiZr_3$ at increasing of the regularization parameter; curves (a): least-squares solution. Final curves (d) are compared with results obtained by applying an iterative method (dotted lines) [5].

acceptable behaviour, while the Ni–Zr and Ni–Ni PDFs are affected by strong unphysical negative features and the typical mirror effect. This is the case of the erroneous situation where a positive strong peak present in a PSF is compensated by a negative peak in another PSF. By increasing λ (from a to d curves), these unphysical features are practically eliminated. Each function, at the best λ value (curves d, full line), is compared with the corresponding function obtained by using an iterative method (curves d, dotted line) [5].

While the Zr-Zr PDFs exhibit a is very good agreement, some comments are necessary for the Ni–Ni and Ni–Zr PDFs. In the case of the regularized Ni–Ni PDFs the short and medium range order apper completely destroyed, while the same PDFs obtained by the iterative method exhibit strong oscillations in the medium range. Really, the absence or the very small Ni–Ni coordination, in amorphous $NiZr_2$ and $NiZr_3$, has been stated by EXAFS [27] and X-ray diffraction [28] investigations, thus the features in the medium

range appear unusual. This result can be interpreted as due to a residual mirror effect between the Ni–Ni and Ni–Zr PDFs, considering that the amplitudes of the oscillations in the medium range of the Ni–Ni and Ni–Zr PDFs are very large, and the positions of the maxima in the Ni–Ni PDFs roughly correspond to the positions of the minima in the Ni–Zr PDFs, and viceversa. In the light of these results, the regularization algorithm seems able to provide reliable PSFs.

2.3.2. Reverse Monte Carlo (RMC)

The reverse Monte Carlo method has been proposed as a method for obtaining a three-dimensional model of the structure of disordered materials from scattering data [29].

The RMC is a variation of the standard Metropolis Monte Carlo procedure (no interatomic potentials are required) in which a structural function calculated from the configuration of the atomic coordinates is systematically compared with the same function obtained by an experiment. The squared difference between the experimental, $F_e(x)$, and calculated, $F_c(x)$, structural function in the real or the reciprocal space is minimized until convergence is reached. With adequate computer time a good agreement is usually obtained. For a binary amorphous material the RMC method can be able to provide the three PSFs, $a_{ij}(q)$, (or the PDFs, $g_{ij}(r)$) using, as input information one or more experimental functions. Only the chemical composition, the measured density of the sample and the closest approach distance of two atoms are needed in the RMC algorithm.

The following steps elucidate the procedure:

i) An initial configuration of N particles in a periodic cubic box of side length L is created. The size of the box must be chosen such that the number density corresponds to the experimental one. The starting configuration may be a lattice, a random network or the result of an earlier simulation.

ii) Starting simulated $g_{ij}(r)$ functions are calculated, and from them any function $F_c(x)$ of interest can be constructed. $F_c(x)$ is compared with the corresponding experimental function $F_e(x)$, via a standard χ^2-test:

$$\chi^2 = \sum_k [F_c(x_k) - F_e(x_k)]^2 / 2\sigma_k^2 , \qquad (18)$$

where σ_k is the estimated experimental error.

iii) A new configuration is generated by a random motion of a randomly chosen particle. This produces a new $F_c(x)$, and a χ'^2 can be calculated.

iv) If $\chi^2 > \chi'^2$, the move is accepted, otherwise it is accepted with a probability $\exp(\chi'^2 - \chi^2)$. The procedure is repeated from (iii).

As the procedure is iterated, χ^2 will decrease to an equilibrium value about which it will oscillate. At this point it is possible to start collecting a set of independent configurations consistent with the experimental data and calculate the average $F_c(x)$. From the three-dimensional model of the atomic positions it is possible to deduce structural information not directly available from diffraction experiments such as the bond angle distribution, defined as the number of angles θ between the two vectors joining a central atom with any two neighbours of its first coordination shell.

3. Experimental and Data Analysis

3.1. Sample Preparation and Characterization

The amorphous CuZr alloy was prepared by milling a suitable mixture of the elemental powders. The milling process was carried out under argon atmosphere using steel vials mounted on a high energy planetary ball mill. The changes to the amorphous phase were monitored by X-ray diffraction spectra taken on small portions of the powder at different milling steps. After 20 h, the crystalline peaks of elemental Cu and Zr have completely disappeared and only a broad halo typical of the amorphous state was present in the spectrum. Fe contamination from the ball mill was found to be less then 2% in the final product.

3.2. X-Ray Diffraction Measurements

The X-ray diffraction data were collected on the wiggler beam line at LURE-DCI (France) using a two-circle goniometer. The powder sample was placed in a vacuum chamber to avoid air scattering contribution to the measured signal. The experimental apparatus is equipped with a two crystal Si (220) monochromator and a Solid State multidetector composed of 12 Si:Li plates [30]. The use of the multidetector has greatly reduced the time needed to reach a good signal/noise ratio.

The energy resolution of the multidetector is sufficient to resolve the fluorescence K_α but not the fluorescence K_β, when the energy of the incident beam is close to that of an absorption K-edge. Moreover, part of the Compton scattered intensity cannot be separated, particularly at low scattering angles.

Table 1. Anomalous scattering factors (electrons) calculated at the different energy values (keV) [33].

Energy	f'_{Cu}	f''_{Cu}	f'_{Zr}	f''_{Zr}
$E_1 = 8.779$	−3.47	0.50	−0.44	1.93
$E_2 = 8.975$	−7.83[a]	1.66[a]	−0.47	1.85
$E_3 = 11.000$	−0.60	2.78	−0.80	1.29
$E_4 = 17.400$	0.24	1.27	−3.02	0.56
$E_5 = 17.990$	0.25	1.20	−7.56[a]	0.99[a]
$E_6 = 18.972$	0.26	1.09	−2.16	3.38

[a] Values obtained from experimental absorption data by means of the optical theorem and the Kramers-Kronig integration [31, 32].

For a binary compound, three different measurements should be, in theory, sufficient to obtain the three PSFs. However, six experiments were performed to reduce the ill-conditioning of the system, allowing also the use of the differential structure factors [21]. The six different photon energies, reported in Table 1, have been suitably chosen to yield significant changes in the real part, f', of the anomalous scattering factors.

The energies E_2 and E_5 are very close the K-edge of Cu (8.980 keV) and Zr (17.998 keV), respectively, and have been selected below the edge in order to reduce the emission of fluorescence. The energies E_1 and E_4 have been selected far enough from the edge to yield a significant variation in f', but not too far in order to take advantage of the cancellation of systematic errors in calculating DSF_{Cu} and DSF_{Zr}. The energies E_3 and E_6 have been chosen far from both edges to evaluate the experimental ratio K_α/K_β for both Cu and Zr, in order to be able to subtract the K_β contribution from the measured data at the energy closest to the K-edge.

3.3 Data Analysis

Great care was necessary in the preliminary steps of data analysis, in particular in the rejection of the K_β fluorescence, the subtraction of Compton scattering and the normalization to obtain the absolute scattering per atom. For the energies nearest to the Cu and Zr K-edge, the values of f'_{Cu} and f'_{Zr}, respectively, were calculated using the Kramers-Kronig relationship [31, 32], starting from experimental absorption data; otherwise tabulated values were used [33]. A full description of the data analysis steps can be found in [5, 23].

Each data set was independently processed to obtain the TSF. These functions were separately analyzed to check their quality and their compatibility. After the rejection of bad data sets, the remaining sets were averaged. According to the Faber-Ziman formalism [14], the total structure factor is obtained from the coherently scattered intensity per atom, $I_c(q, E)$:

$$a(q, E) = [I_c(q, E) - (\langle f^2 \rangle - \langle f \rangle^2)]/\langle f \rangle^2 , \quad (19)$$

$$\langle f^2 \rangle = c_A f_A f_A^* + c_B f_B f_B^* . \quad (20)$$

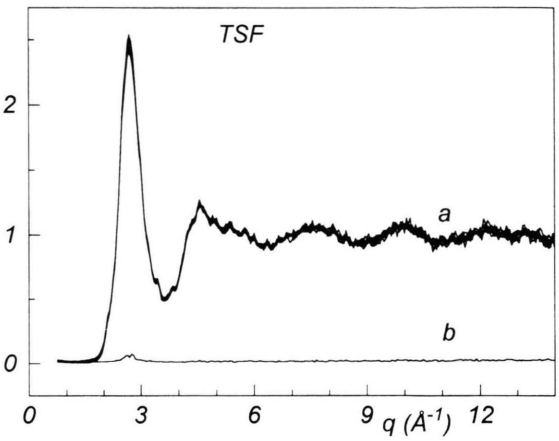

Fig. 3. (a) Superimposition of ten different total structure factors measured at the energy $E_5 = 17.990$ keV by ten different detectors. (b) Standard deviation calculated by averaging 20 measurements at the same energy.

Figure 3 shows how ten different TSFs measured at the energy $E_5 = 17.990$ keV by ten different detectors superimpose very well after all steps of data reduction. In the same figure, the standard deviation from 20 measurements at the same energy value is also reported.

4. Results

4.1. Total Structure Factors

The six TSFs corresponding to the chosen energies are shown in Figure 4. Some considerations can be made. (i) The differences among the averaged TSFs are small due to the small values of f' and f'' with respect to f^0. (ii) The curves exhibit a very good signal/noise ratio which is mostly due to the implementation of the multidetector. (iii) Due to the preparation method small crystalline contributions are present in the spectra [23, 34]. Thus, some features in the TSFs are due to crystalline peaks only ascribable to residual metallic Cu and Zr since no trace of oxide or

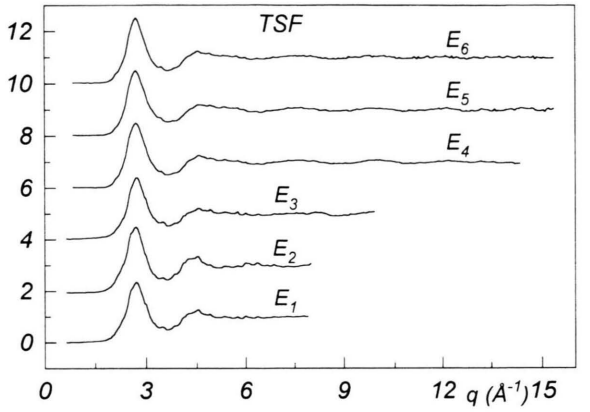

Fig. 4. Total structure factors, $a(q, E)$, corresponding to the six energies used: (E_1) 8.779 keV, (E_2) 8.975 keV, (E_3) 11.000 keV, (E_4) 17.400 keV, (E_5) 17.990 keV and (E_6) 18.972 keV. To better compare their behaviour, curves from (E_2) to (E_6) have been conveniently shifted upwards.

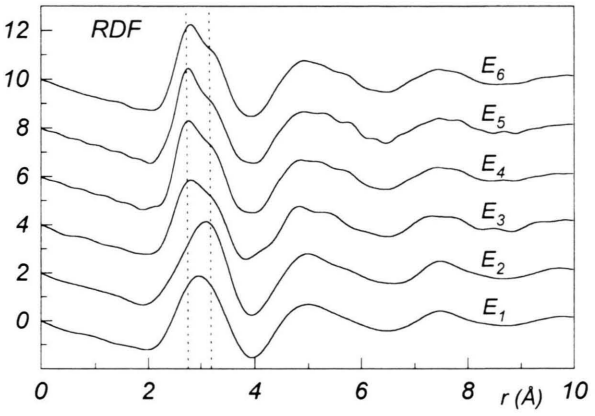

Fig. 5. Radial Distribution Functions calculated by Fourier transforming the six TSFs reported in Figure 4. The two distances Cu–Cu/Cu–Zr and Zr–Zr are roughly evidenced (dashed lines).

intermetallic crystalline phases was observed. In any case, the estimated amount of crystalline contribution should not significantly modify the composition of the amorphous phase. The main evidencies of the crystalline residual phases can be observed on both sides of the main peak and also at about 3.50 Å^{-1} and in the range from 4.5 to 6 Å^{-1}. To undoubtedly attribute these features we observed how they change when the differential structure factors are calculated. All contributions not involving Cu and Zr atoms are, in fact, eliminated in the DSF_{Cu} and DSF_{Zr}, respectively.

It must be pointed out, however, that the presence of residual crystallinity is not a crucial point. In fact, we performed in the following two parallel data treatments (with and without removing the crystalline contributions) obtaining two sets of PSFs which exhibit the same shape. Only very small bumps remain in the uncorrected set at the same q-points where the TSFs are affected by the residual crystalline contributions.

In the real space, the effects of the crystalline contributions in the RDFs calculated by Fourier transforming the total structure factors are not appreciable at all. The six RDFs, reported in Fig. 5, show different shapes in the region of the first peak due to the differences in the weighting factors w_{ij}. The left side of the peak (shorter distances) is enhanced when the contribution of the pairs containing Zr are lower, i.e. at the energies E_4, E_5, E_6 nearest to the Zr K-edge. On the contrary, when the energies are close to the Cu K-edge, i.e. E_1, E_2, E_3, the pairs containing Cu contribute less to the RDFs, and the asymmetry of the first peak is shifted towards larger distances. Going from lower to higher r values, the distance Cu–Cu and Cu–Zr and the distance Zr–Zr are therefore evidenced.

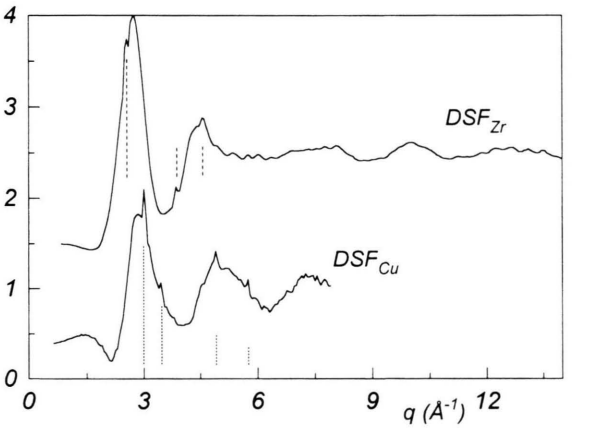

Fig. 6. Differential structure factors relative to Cu K-edge, ($E_1 = 8.779$ and $E_2 = 8.975$ keV), and Zr K-edge ($E_4 = 17.400$ and $E_5 = 17.990$ keV). Diffraction lines of crystalline Cu (dotted lines) and Zr (dashed lines) are also reported (arbitrary units).

4.2. *Differential Anomalous Scattering*

The two pairs of energies $E_1 - E_2$ and $E_4 - E_5$ were used to evaluate DSF_{Cu} and DSF_{Zr}, respectively. These functions are reported in Fig. 6 together with the characteristic features of the crystalline Cu and Zr

whose diffraction lines are drawn in an arbitrary scale. As expected, crystalline contributions appear in each DFS: in DSF_{Cu} the peaks at 3.00, 3.50, 4.90, and 5.75 $Å^{-1}$ coincide with the positions of (111), (200), (220) and (311) diffraction lines of elemental Cu. These peaks are absent in DSF_{Zr}, while three peaks at 2.55, 3.90 and 4.60 $Å^{-1}$, not present in DSF_{Cu}, emerge due to (101), (110) and (112) diffraction lines of elemental Zr. As pointed out, we have estimated that the amounts of the crystalline phases are approximately equal, not affecting considerably the composition of the amorphous phase.

The precise evaluation of the position of the crystalline peaks allowed us to remove these contributions from each TSF and DSF in the following way: i) the crystalline peaks were first eliminated from DSF_{Cu}, (DSF_{Zr}) and from the TSF at the energy E_2 (E_5), the nearest to Cu (Zr) K-edge, where these effects are more enhanced; ii) the TSF at the energy E_1 (E_4), has been re-calculated, from the pair of functions DSF_{Cu} and the TSF at the energy E_2, (DSF_{Zr} and the TSF at E_5) to have a self-consistent set of corrected functions. A similar procedure has been applied to remove the crystalline contributions from the TSFs at the energies E_3 and E_6, i.e. two more DSFs (one around the Cu and the other around the Zr, respectively) were calculated using the pairs of energies E_2-E_3 and E_4-E_6.

The DSFs thus corrected are reported in Figure 7. Nearest neighbour distances and coordination numbers have been obtained from a profile analysis in real space of the first peak of each differential distribution function. It can be expressed as a sum of two Gaussian distributions, i.e., Cu–Cu and Cu–Zr distances for DDF_{Cu} and Zr–Cu and Zr–Zr distances for DDF_{Zr}. Figure 8 shows the agreement between experimental and calculated DDFs. Best fit values for the structural parameters are reported in Table 2.

4.3. *Partial Structure Factors*

As a first approach, we tried to solve the system by involving three (corresponding to the energies E_1, E_2, and E_5) and six (including the energies E_3, E_4, and E_6) TSFs and using a least square routine. The conditioning numbers cond (W) for these two combinations are reported in Figure 9. No reliable solutions were found in this way.

The introduction in the system of the four DSFs gave rise to a strong improvement but was not sufficient to provide a set of solutions unaffected by distor-

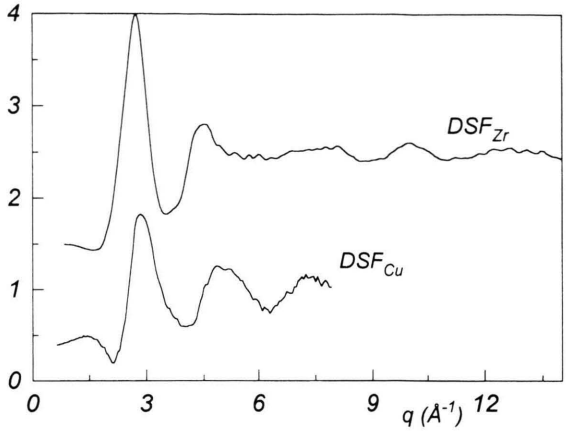

Fig. 7. Differential structure factors (see Fig. 6) after removal of the residual crystalline contributions.

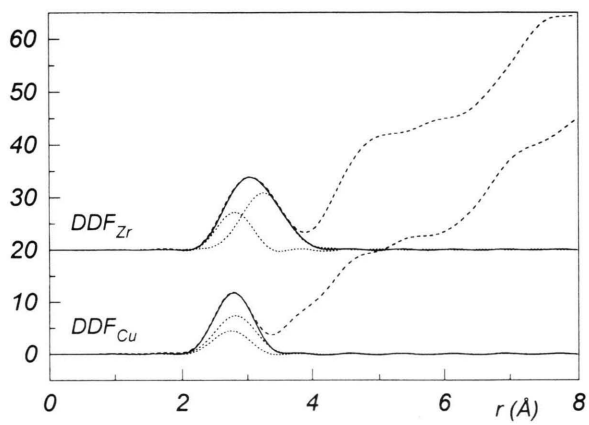

Fig. 8. Profile fitting in real space (full lines) of the first peak in experimental DDF_{Cu} and DDF_{Zr} (dashed lines). The two Gaussian contributions are also reported (dotted lines).

Table 2. Distances, R(Å), and coordination numbers, N (atoms), obtained fitting the first shell in real space for both DDF_{Cu} [a] and DDF_{Zr} [b]. Estimated uncertainties are $\Delta R = \pm 0.03$ Å and $\Delta N = \pm 0.5$ atoms.

	R	N
Cu–Cu [a]	2.69	4.20
Cu–Zr [a]	2.79	4.50
Zr–Cu [b]	2.79	4.80
Zr–Zr [b]	3.22	8.50

sions. The Fig. 10 shows the PSFs obtained by solving the system in the least-square sense. The three PSFs clearly show distorsion due to the mirror effect, especially at low q-values, where the conditioning number is higher. In real space, the three PDFs too exhibit

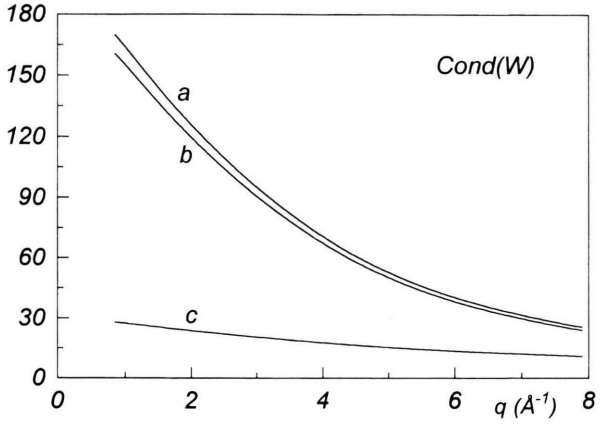

Fig. 9. Behaviour of the conditioning number, cond(W), when (a) Three (E_1, E_2, E_5) and (b) six (including E_3, E_4, E_6) total structure factors are used in the system to obtain the partial structure factors. Curve (c) shows the considerable decrease of cond(W) when the four differential structure factors are introduced in the systsem.

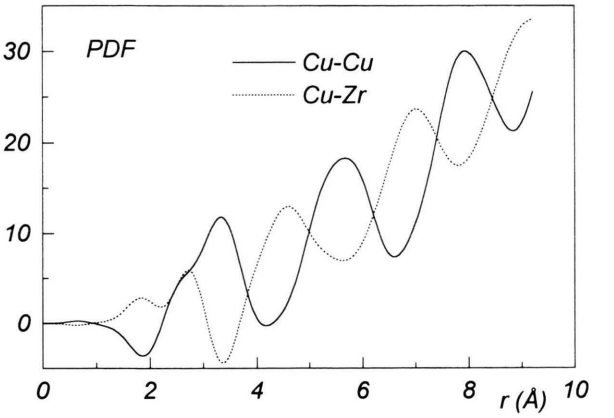

Fig. 11. Cu–Cu and Cu–Zr partial distribution functions (least squares solution). The *mirror effect* between these two smaller contributions to the measured TSFs is clearly shown.

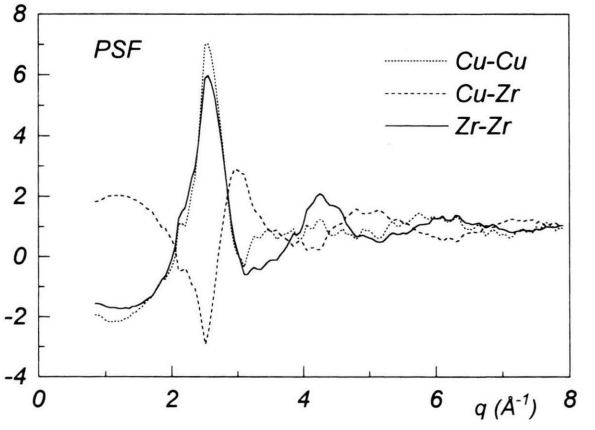

Fig. 10. Partial structure factors obtained by solving the system (12) in the least-squares sense.

unphysical values in large intervals: while the Zr–Zr pair shows a physically meaningful behaviour, the Cu–Zr and Cu–Cu PDFs suffer from the mirror effect as shown in Figure 11. In particular the unphysical peak at 3.35 Å in the Cu–Cu PDF is counterbalanced by a negative peak in the Cu–Zr PDF. This behaviour can be explained by the largest contribution of the Zr–Zr pair to the TSFs, while the Cu–Cu and Cu–Zr pairs are the minor components and thus they are subject to larger errors.

We have tryed to solve the system by using different combinations of input functions and changing the set of the weighting factors, but these attempts all failed. On the contrary, the regularization algorithm described in the first section gave reliable PDFs. The strategy was to vary the regularization parameter, starting from $\lambda = 0$ (least-squares solution) until no negative values were present in the PDFs. Figure 12 shows the evolution of the behaviour of the three PDFs: by increasing the regularization parameter λ, the mirror effect and the regions with negative values have been progressively reduced, and finally (curves d) they disappeared. When λ is increased above this optimal situation, the solutions became worse until they did not change significantly: the three PDFs obtained with this upper value of λ are reported in Figure 13. Note that the Cu–Cu pairs shows a lower minimum below zero after the first peak, while the first peak in the Cu–Zr pair becomes less definite. A similar behaviour is present in the PDFs of a $Cu_{46}Zr_{54}$ amorphous sample [9] prepared by melt-spinning. The latter are obtained by anomalous X-ray scattering data through a different approach based on the Bhatia-Thornton formalism [35]. The comparison between the curves in Fig. 13 suggests a not complete absence of the mirror effect in the procedure proposed.

4.4 Reverse Monte Carlo

The RMC method has been applied to experimental data for extracting an independent set of three PDFs. The fitting procedure has been carried out in real space

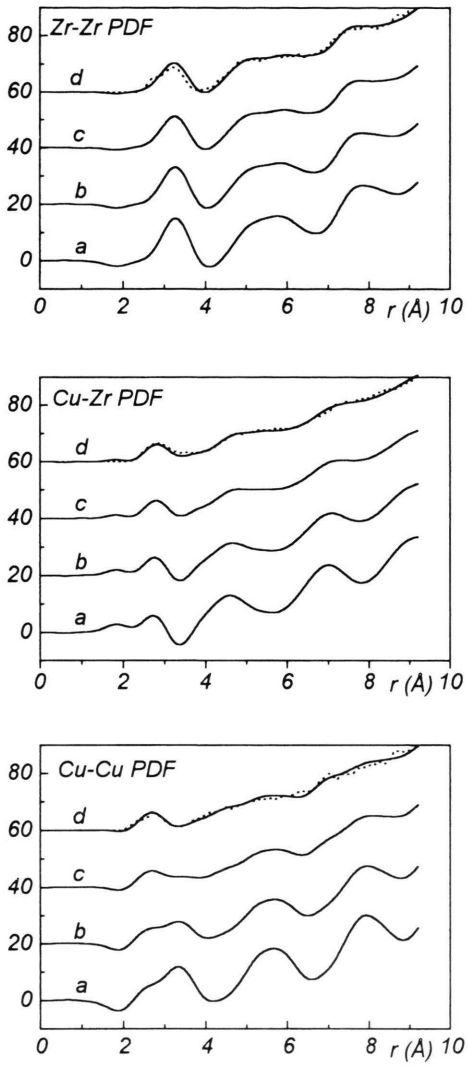

Fig. 12. Partial distribution functions for the amorphous CuZr at increasing of the regularization parameter; curves (a): least-squares solution. Final curves (d) are compared with results obtained by applying the RMC method (dotted lines).

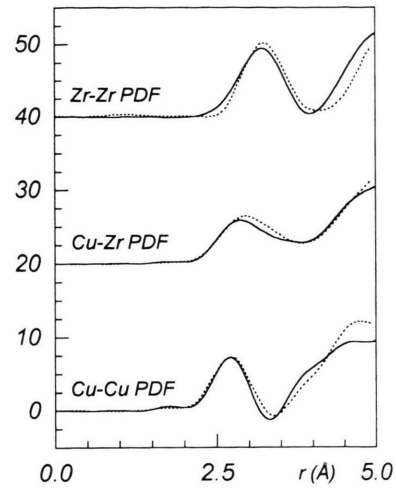

Fig. 13. The three partial distribution functions, obtained by increasing λ above its optimal value (full lines), compared with those obtained for the amorphous $Cu_{54}Zr_{46}$ prepared by melt spinning technique (dotted lines) [9].

using, as input functions, the two differential distribution functions obtained from the TSFs at the energies $E_1 - E_2$ and $E_4 - E_5$, and the RDF at $E_5 = 17.990$ keV.

A cubic box of 1000 randomly distributed atoms was used as starting configuration for the fitting procedure. The side of the box was fixed $L = 26$ Å for taking into account the experimental density. From the behaviour of the RDF and the DDFs, the cut-off distances have been set to: $r_{CuCu} = 2.1$ Å, $r_{CuZr} = 2.2$ Å and $r_{ZrZr} = 2.2$ Å.

The three PDFs thus obtained are compared, in Fig. 12 with those calculated by the AXS method at the best regularization parameter (curves d). The agreement between the two sets of results is quite satisfactory.

To characterize the local orientational order, a set of rotational invariants Q_l of spherical harmonics may be evaluated [36]. The Q_l shave been calculated taking into account clusters of about thirteen atoms made up by a central atom surrounded by its nearest neighbours. They indicate that the preferred local symmetry corresponds to a hexagonal close packed distribution of atoms with a 20% degree of disorder [37]. The six bond angle distribution functions exhibit very similar behaviour with two maxima at 60° and 110°, showing no particular preference for the coordination among unlike atom pairs.

5. Discussion

Two sets of PDFs have been independently obtained by the AXS and RMC method. From them structural information such as R_{ij}, N_{ij} and η_{ij} can be evaluated, these results are reported in Table 3. We can readily see that the two sets compare well, and the values of the structural parameters are in agreement with those obtained by profile fitting the two DDFs.

Table 3. First distances (R_{ij}) and coordination numbers (N_{ij}) compared with structural parameters from literature.

	Method	Ref.	R_{ij}(Å)			N_{ij}(atoms)			η (η_{ZrCu})
			CuCu	CuZr	ZrZr	CuCu	CuZr	ZrZr	
$Cu_{50}Zr_{50}$	AXS *		2.68	2.80	3.16	4.6	4.8	7.8	−0.10
$Cu_{50}Zr_{50}$	RMC *		2.64	2.78	3.14	4.3	5.5	7.0	0.00
$Cu_{50}Zr_{50}$	AXS	[11]	2.53	2.75	3.15	5.8	5.6	5.0	0.019
$Cu_{46}Zr_{54}$	AXS	[9]	2.63	2.81	3.20	4.7	5.3	7.7	−0.10
$Cu_{57}Zr_{43}$	NDIS	[12]	2.65	2.80	3.15	5.4	5.0	5.9	0.014
$Cu_{57}Zr_{43}$	NDIS	[13]	2.59	2.77	3.28	8.2	5.1	5.2	−0.056

* Estimated uncertainties are $\Delta R = \pm 0.03$ Å, $\Delta N = \pm 0.5$ atoms and $\Delta\eta = \pm 0.03$. (NDIS = Neutron Diffraction with Isotopic Substitution).

Therefore, in spite of the difficulties in obtaining the PDFs, they can be considered physically reasonable.

In Table 3 the results obtained by other authors on the CuZr system, prepared by melt spinning technique, are also reported. We note that the agreement between the atomic distances is quite satisfactory while larger differences are observed on some coordination numbers. Indeed N_{ij} values are more affected by errors during the solution procedures; furthermore, different compositions may reflect on different atomic coordinations. The presence of chemical short range order is an important question to correctly describe the structure of metal-metal alloys. The order parameter η_{ZrCu}, calculated following (8) show a weak chemical order tendency. Little discrepancies in the values of η_{ZrCu} are found in literature and may be ascribed to the difficulties in the determination of reliable partial coordination numbers. The uncertainties in N_{ij} make it hard to demonstrate an unquestionable evidence of a chemical short range order in case of small negative values of η_{AB} [13].

Within these considerations, the samples of amorphous CuZr prepared by mechanical alloying and melt spinning technique exhibit similar atomic scale structure.

6. Conclusion

In this work we have shown that the AXS technique can be successfully applied in the study of amorphous binary compounds prepared by mechanical alloying. Sometimes, due to the preparation method, crystalline peaks from residual elemental powders are present in the measured data. In the best case of small contributions these peaks can be eliminated. If an absorption edge of both atomic species is accessible, it is possible to obtain important structural information making use of the differential structure factors. A regularization method has been presented to minimize errors and spurious effects in the determination of the three partial structural factors. This method displays good properties of stability with respect of random and, sometimes, systematic errors. Unfortunately, the systematic errors cannot be, in principle, successfully treated with the available regularization methods. They can be better approached by solving a system of integral equations where the unknown functions are represented directly by the PDFs. Moreover, physical constraints and a priori information about the behaviour of the PDFs (i.e. asymptotic behaviour, non negativity, absence of ripples in the low r region) could be introduced into the regularization procedure.

The RMC algorithm has demonstrated to be a powerful tool for obtaining a three-dimensional model of metal-metal amorphous alloys where no noticeable preferred coordinations among unlike atom-pairs is evidenced. The PDFs obtained by this method are very close to those obtained by the regularization algorithm.

The comparison of the structural parameters of amorphous samples prepared by different techniques may support the idea of an underlying *ideal glass state* to which the real glasses, obtained in non-ideal conditions, may be referred. Of course, to deeper elucidate this very delicate questions, further study is necessary.

This work is part of the research program "Progetto Finalizzato Materiali Speciali per Tecnologie Avanzate", Consiglio Nazionale delle Ricerche (CNR, Italy).

[1] A. C. Wright, J. Non-Cryst. Solids **106,** 1 (1988).
[2] D. Raoux, in: Proc. ILL/ESRF Workshop on Methods in the Determination of Partial Structure Factors of Disordered Matter by Neutron and Anomalous X-Ray Diffraction, Grenoble 1992 ed. J. B. Suck, P. Chieux, D. Raoux, and C. Riekel, World Scientific, Singapore 1993, p. 130.
[3] J. E. Enderby, in: Proc. ILL/ESRF Workshop on Methods in the Determination of Partial Structure Factors of Disordered Matter by Neutron and Anomalous X-Ray Diffraction, Grenoble 1992 ed. J. B. Suck, P. Chieux, D. Raoux, and C. Riekel, World Scientific, Singapore 1993, p. 16.
[4] P. H. Fuoss, P. Eisenberger, W. K. Warburton, and A. Bienenstock, Phys. Rev. Lett. **46,** 1537 (1981).
[5] J. C. de Lima, Ph.D. thesis, Université de Paris-Sud (1989).
[6] Y. Waseda, The Structure of Non-Crystalline Materials, McGraw-Hill, London 1980.
[7] G. Licheri, G. Navarra, and S. Seatzu, J. Non-Cryst. Solids **119,** 29 (1990).
[8] Yu. A. Babanov, R. Sh. Sadykova, V. R. Shvetsov, A. V. Serikov, A. L. Ageev, and V. V. Vasin, J. Non-Cryst. Solids **119,** 159 (1990).
[9] G. H. Bezerra, L. Q. Amaral, A. F. Craievich, and D. Raoux, J. Non-Cryst. Solids **126,** 239 (1990).
[10] M. Bionducci, F. Buffa, G. Licheri, and G. Navarra, in: Proc. ILL/ESRF Workshop on Methods in the Determination of Partial Structure Factors of Disordered Matter by Neutron and Anomalous X-Ray Diffraction, Grenoble 1992 ed. J. B. Suck, P. Chieux, D. Raoux, and C. Riekel, World Scientific, Singapore 1993, p. 151.
[11] H. S. Chen and Y. Waseda, Phys. Stat. Sol. **A 51,** 593 (1979).
[12] T. Misoguchi, T. Kudo, T. Irisawa, N. Watanabe, N. Niimura, M. Misawa, and K. Suzuki, in: Proc. 3rd Int. Conf. on Rapidly Quenched Metals, ed. B. Cantor, The Metal Society, London 1978, p. 384.
[13] P. Lamparter, S. Steeb, and G. Grallath, Z. Naturforsch. **A 38,** 1210 (1983).
[14] T. E. Faber and J. M. Ziman, Philos. Mag. **11,** 153 (1965).
[15] B. E. Warren, X-Ray Diffraction, Addison-Wesley, Reading, MA, 1969.
[16] M. Magini, G. Licheri, G. Piccaluga, G. Paschina, and G. Pinna, X-Ray Diffraction of Ions in Aqueous Solutions: Hydration and Complex Formation, CRC, Boca Raton, FL, 1988.
[17] G. S. Cargill and F. Spaepen, J. Non-Cryst. Solids **43,** 91 (1981).
[18] G. Licheri and G. Pinna, Soc. Ital. Fis. Conf. Proc. **25,** 585 (1990).
[19] G. H. Golub and C. F. Van Loan, Matrix Computation, North Oxford Academy, Oxford 1983.
[20] J. Stoer and R. Bulirsch, Introduction to Numerical Analysis, Springer, Berlin 1980.
[21] R. G. Munro, Phys. Rev. **B 25,** 5037 (1982).
[22] K. F. Ludwig Jr., W. K. Warburton, L. Wilson, and A. I. Bienenstock, J. Chem. Phys. **87,** 604 (1987).
[23] F. Buffa, A. Corrias, G. Licheri, G. Navarra, and D. Raoux, J. Non-Cryst. Solids **151,** 119 (1992).
[24] Q. Ma, Ph.D. thesis, Université de Paris-Sud (1992).
[25] Yu. A. Babanov, R. Sh. Sadykova, V. R. Shvetsov, A. V. Serikov, A. L. Ageev, and V. V. Vasin, Nucl. Instrum. Methods Phys. Res. **A 282,** 646 (1989).
[26] G. Navarra, M. Bionducci, F. Buffa, and G. Licheri, in: Proc. ILL/ESRF Workshop on Methods in the Determination of Partial Structure Factors of Disordered Matter by Neutron and Anomalous X-Ray Diffraction, Grenoble 1992 ed. J. B. Suck, P. Chieux, D. Raoux, and C. Riekel, World Scientific, Singapore 1993, p. 155.
[27] R. Frahm, R. Haensel, and P. Rabe, J. Phys. F: Met. Phys. **14,** 1333 (1984).
[28] F. Paul and R. Frahm, Phys. Rev. **B 42,** 10945 (1990).
[29] R. L. McGreevy and L. Pusztai, Mol. Sim. **1,** 359 (1988).
[30] G. Nicoli, R. Andouart, C. Barbier, D. Dagneaux, M. De Sanctis, and D. Raoux, Soc. Ital. Fis. Conf. Proc. **25,** 353 (1990).
[31] P. Dreier, P. Rabe, W. Malzfeldt, and W. Nieman, J. Phys. **C 17,** 3123 (1984).
[32] J. J. Hoyt, D. de Fontaine, and W. K. Warburton, J. Appl. Cryst. **17,** 344 (1984).
[33] S. Sasaki, KEK Report 83-22, Nat. Lab. for High Energy Phys., Tsukuba, Japan 1984.
[34] M. S. Boldrick and C. N. J. Wagner, Mater. Sci. Eng. **A 134,** 872 (1991).
[35] A. B. Bhatia and D. E. Thornton, Phys. Rev. **B 2,** 3004 (1970).
[36] P. J. Steinhardt, D. R. Nelson, and M. Ronchetti, Phys. Rev. **B 28,** 784 (1983).
[37] M. Bionducci, F. Buffa, G. Licheri, and G. Navarra, in: Proc. ILL/ESRF Workshop on Methods in the Determination of Partial Structure Factors of Disordered Matter by Neutron and Anomalous X-Ray Diffraction, Grenoble 1992 ed. J. B. Suck, P. Chieux, D. Raoux, and C. Riekel, World Scientific, Singapore 1993, p. 229.